AD_____

Award Number: DAMD17-03-1-0119

TITLE: Ultrasound Activated Contrast Imaging for Prostate Cancer Detection

PRINCIPAL INVESTIGATOR: Flemming Forsberg, Ph.D.

CONTRACTING ORGANIZATION: Thomas Jefferson University
Philadelphia, Pennsylvania 19107

REPORT DATE: March 2007

TYPE OF REPORT: Final

PREPARED FOR: U.S. Army Medical Research and Materiel Command
Fort Detrick, Maryland 21702-5012

DISTRIBUTION STATEMENT: Approved for Public Release;
Distribution Unlimited

REPORT DOCUMENTATION PAGE

Form Approved
OMB No. 0704-0188

1. REPORT DATE *(DD-MM-YYYY)*	**2. REPORT TYPE**	**3. DATES COVERED** *(From - To)*
01/03/07	Final	1 Mar 2003 – 28 Feb 2007

4. TITLE AND SUBTITLE

Ultrasound Activated Contrast Imaging for Prostate Cancer Detection

5a. CONTRACT NUMBER

5b. GRANT NUMBER
DAMD17-03-1-0119

5c. PROGRAM ELEMENT NUMBER

6. AUTHOR(S)
Flemming Forsberg, Ph.D.

E-Mail: Flemming.Forsberg@jefferson.edu

5d. PROJECT NUMBER

5e. TASK NUMBER

5f. WORK UNIT NUMBER

7. PERFORMING ORGANIZATION NAME(S) AND ADDRESS(ES)

Thomas Jefferson University
Philadelphia, Pennsylvania 19107

8. PERFORMING ORGANIZATION REPORT NUMBER

9. SPONSORING / MONITORING AGENCY NAME(S) AND ADDRESS(ES)
U.S. Army Medical Research and Materiel Command
Fort Detrick, Maryland 21702-5012

10. SPONSOR/MONITOR'S ACRONYM(S)

11. SPONSOR/MONITOR'S REPORT NUMBER(S)

12. DISTRIBUTION / AVAILABILITY STATEMENT
Approved for Public Release; Distribution Unlimited

13. SUPPLEMENTARY NOTES

14. ABSTRACT: The current project proposes todevelop a novel ultrasound contrast imaging technique (called EEI) for better visualization of the microvessels, which are characteristic of the neovasculature associated with prostate cancer. In vitro, Sonazoid produced 10dB of enhancement at 22°C, which reduced to 5dB at 37°C. Conversely, Optison created 1dB of enhancement at 22°C, which increased to 9dB at 37°C. This enhancement reduced to 3dB when the concentration was increased from 0.05 to 0.5µl/l. While no enhancement was found for Definity at any of the concentrations studied, QFX produced approximately 17 and 14dB of enhancement at the fundamental and harmonic frequencies, respectively. Initial simulation results indicate that the shell elasticity plays a vital role in the growth as well as dissolution of the bubbles. While results at an imaging frequency of 7.5MHz were somewhat in agreement with measurements, the enhancement was unrealistically high (20-35dB). Somewhat disappointingly only 1-4dB of enhancement was produced by EEI in vivo. In conclusion, up to 17dB of enhancement can be achieved with EEI in vitro. However, EEI appears to be quite sensitive to changes in temperature and microbubble concentration, which may explain the reduced enhancement observed in vivo.

15. SUBJECT TERMS
Prostate Cancer, Ultrasound Imaging, Ultrasound Contrast Agent

16. SECURITY CLASSIFICATION OF:			**17. LIMITATION OF ABSTRACT**	**18. NUMBER OF PAGES**	**19a. NAME OF RESPONSIBLE PERSON**
a. REPORT	**b. ABSTRACT**	**c. THIS PAGE**			USAMRMC
U	U	U	UU	28	**19b. TELEPHONE NUMBER** *(include area code)*

3. TABLE OF CONTENTS

4. INTRODUCTION

The diagnosis of prostate cancer is currently based on an elevated prostate-specific antigen (PSA) level or abnormal digital rectal examination findings confirmed by needle biopsy of the prostate. It is estimated that the number of men subjected to biopsy of the prostate in the U.S. in 2001 exceeded 600,000 [1]. Unfortunately, the frequency of positive biopsy findings, for most screening populations, was as low as one in three to one in four. Therefore, an accurate, noninvasive diagnostic imaging examination of the prostate is needed to reduce the number of biopsies or even to replace biopsy.

A sextant biopsy of the prostate, consisting of the acquisition of six biopsy cores, can miss clinically detectable prostate caner in up to 34% of men. Among patients with an elevated PSA level and a negative initial sextant biopsy finding, repeat biopsy demonstrates the presence of malignancy in approximately 20%-30% [2]. However, each additional biopsy is associated with a small incremental risk of hemorrhage and infection. Thus, an accurate, noninvasive imaging technique is useful for targeted biopsy guidance in order to reduce the number of biopsies in each prostate.

The sensitivity and specificity of ultrasound imaging can be improved by intravenous injection of vascular contrast agents consisting of encapsulated gas microbubbles [3]. Due to encapsulation, these agents are stable enough to pass through the pulmonary circulation and flow in intravascular space for at least several minutes. However, encapsulation imposes severe restrictions on the oscillations of contrast bubbles. Based on de Jong's numerical model [4], our calculations indicate that the incident acoustic pressure amplitude for an albumin-encapsulated Abunex® bubble is 18 times greater than that for a free bubble if the two bubbles oscillate with the same relative amplitude at their resonant frequency of 2 MHz. Hence, scattering can be greatly enhanced if encapsulated bubbles become free bubbles. According to the Rayleigh's approximation, the fundamental scattering cross-section of an air bubble is more than 200 times (47 dB) greater than that for an Abunex bubble of the same size. Furthermore, the enhancement in second or sub- harmonic scattering cross-section must be even much greater because encapsulation dampens nonlinear oscillations to a much greater degree.

Unlike current ultrasound imaging modalities employing only an imaging field, the proposed technique utilizes two acoustic fields: the activation field for intermittently activating contrast bubbles and the imaging field, applied shortly afterwards, for acquiring harmonic or subharmonic images with significantly enhanced scattering signals from activated contrast bubbles. This new imaging mode is referred to as Excitation Enhanced Imaging (EEI) [5]. Based on previous work on ultrasound-induced contrast scattering enhancement and contrast-assisted ultrasonographic detection of human and canine prostate cancer, the hypotheses of this study are: (1) contrast microbubbles can be ultrasonically activated to achieve marked backscattering enhancement, and (2) the detection of prostate cancer can be improved using the proposed ultrasonographic technique. It is well known that a free bubble resonating at the insonation frequency is the optimal acoustic scatterer. Hence, the activation field will consist of a release pulse for effectively releasing free bubbles from encapsulated contrast bubbles and an excitation pulse for shifting the free bubbles to the resonance size corresponding to a pre-selected imaging frequency.

5. BODY

It is the central hypothesis of this study that contrast microbubbles can be activated and backscattering enhanced markedly. The activation field will produce the optimal acoustic scatterers, i.e., free bubbles resonant around a pre-selected imaging frequency. In the proposed study, both the modeling and measurement will help us to determine optimal contrast agents and develop optimal activation pulse sequences enhancing backscattered second and sub-harmonic signals by a factor of 2 to 16, i.e., by 6 to 24 dB. The other hypothesis of this study is that prostate cancer can be detected using the proposed ultrasonographic technique. This hypothesis will be tested using an established canine prostate tumor model. The specific tasks of the project (as presented in the original Statement of Work) can be found in Appendix I.

First an outline of the methods applied will be given followed by a presentation of the results to date. Finally, the conclusions and future directions of the research will be discussed.

5.1 Methods

Contrast microbubble modeling

The interface of an encapsulated contrast microbubble gives rise to interfacial forces that are modeled by rheology. We have adopted a Newtonian rheology, i.e., only viscous interfacial stresses are considered (see [6] for details). Assuming spherical symmetry (for a micron size bubble in a pressure field of 1 MHz, the radius to wavelength ratio is too small, $\sim 10^{-3}$, to experience substantial shape deformation except for extreme cases of microbubble breakup), the normal (r-component) stress boundary condition at the bubble radius ($r = R$), given by:

$$p(r=R,t) = P_G - 4\mu\frac{\dot{R}}{R} - \frac{4\kappa^s\dot{R}}{R^2} - \frac{2\gamma}{R}. \qquad (1)$$

$p(r=R,t)$ is the pressure in the liquid immediately outside of the bubble, P_G is the uniform gas pressure inside the bubble (Fig 1b), μ the liquid viscosity, κ^s and γ are interfacial dilatational viscosity and surface tension respectively. $\dot{R}$ is the bubble wall velocity while R is the instantaneous bubble radius. The gas pressure inside the bubble is assumed to vary with bubble volume polytropically with k as the polytropic exponent as follows:

$$P_G R^{3k} = P_{G0} R_0^{\,3k}. \qquad (2)$$

P_{G0} is the gas pressure and $R=R_0$ at time $t=0$. Given the boundary condition of eqn. (1) for the liquid-gas system, we obtain the modified Rayleigh-Plesset type equation (for details see [6]):

$$\rho(R\ddot{R} + \frac{3}{2}\dot{R}^2) = P_{G0}\left(\frac{R_0}{R}\right)^{3k} - 4\mu\frac{\dot{R}}{R} - \frac{2\gamma}{R} - \frac{4\kappa^s\dot{R}}{R^2} - P_0 + P_A\sin\omega t, \qquad (3)$$

where, P_0 is the liquid hydrostatic pressure, $\omega=2\pi f$ with f being the driving frequency and P_A is the acoustic pressure amplitude. At $t=0$, $R(t=0)=R_0$, and $\dot{R}(t=0)=0$. Eqn (3) together with these initial conditions describes the bubble dynamics. Note that the third and the fourth terms in the right-hand-side contain the effects of the interface. This model represents the completion of Task 1b as outlined in the original SOW (see the Appendix) and was published as a peer-reviewed paper [7].

The acoustic pressure $P_s(t)$ scattered by a bubble is (in [8], p.83):

$$P_s(r,t) = \rho \frac{R}{r}\left(2\dot{R}^2 + R\ddot{R}\right) \tag{4}$$

Subharmonic component of the scattered signal is determined by transforming this time-domain expression into frequency domain (i.e., $P_s(\omega)$). For comparison, we have also computed similar results for the Church's shell model [9] using the formulation presented by Hoff et al [10] (eqn. (6) in their paper). This model is hereafter referred to as the Church-Hoff model.

Dual pulse EEI with Sonazoid (using size distribution and attenuation data from [10, 11]) was simulated. The PRF used was 2 Hz while 36 and 16 cycles were used for imaging and excitation signals, respectively, with acoustic pressures of 0.1 and 1.2 MPa (i.e., similar to the parameters used for the *in vitro* measurements). The excitation pulse frequency employed was 1.1 MHz and the imaging frequency was either 3.0 MHz or 7.5 MHz. This represents the continuation of task 1c (see original SOW in the Appendix). However, this model did not predict experimental results well (see results below and previous report). Hence, we have attempted to produce a more realistically model incorporating bubble growth and dissolution via rectified diffusion, and these efforts have been presented at an international conference [12].

Here we model the bubble shell as a semi-permeable membrane, with two gases air and octafluoropentane (OFP) inside the bubble. The dissolution time scale and the growth of the bubbles have been studied for varying mole fraction of the osmotic agent (OFP), surface tension, shell permeability, and air saturation level in the bulk. Also, elastic shell has been considered and it has been found that shell elasticity plays a vital role in the dissolution and growth of these bubbles. The dissolution process as said earlier is delayed due to the presence of the shell. Here we assume the process of dissolution to be very slow and hence dissolution by steady diffusion is being considered.

Let the concentration of the gas in the liquid be C. Using the steady state diffusion equation and appropriate boundary conditions allows us to arrive at the following expression:

$$\frac{d(R^3 C_g)}{dt} = 3R^2 k_g \frac{(C_\infty - C_w)}{\left(\frac{k_g}{\alpha} + R\right)} \tag{5}$$

where k_m and k_g are the coefficients of diffusivity of the gas through membrane and the liquid, respectively, while δ is the thickness of the membrane (shell) and α is the ratio of the k_m/δ. The concentration of the gas on the inner and the outer wall of the bubble are $C_w \& C_R$, respectively. If we consider 2 different gases fluorocarbon and air in the bubble, then Eqn (5) can be written as Eqn's (6) and (7) for fluorocarbon (index *F*) and air (index *A*), respectively.

$$\frac{d(R^3 C_F)}{dt} = 3R^2 k_F \frac{(C_{F(\infty)} - C_{F(w)})}{\left(\frac{k_F}{\alpha_F} + R\right)} \tag{6}$$

$$\frac{d(R^3 C_A)}{dt} = 3R^2 k_A \frac{(C_{A(\infty)} - C_{A(w)})}{\left(\frac{k_A}{\alpha_A} + R\right)} \tag{7}$$

After some mathematical manipulations these equations can be reduced to [12]:

$$\frac{dF}{d\tau} = \frac{-3L_F F}{\rho\left(\frac{k_F}{\alpha_F R_o} + \rho\right)} \tag{8}$$

$$\frac{dA}{d\tau} = \frac{-3\xi L_A (A - \rho^3)}{\rho\left(\frac{k_A}{\alpha_A R_o} + \rho\right)} \tag{9}$$

$$F + A = \rho^2(\mu + \rho) \tag{10}$$

where L represents the Ostwald coefficient and the remaining variables are expressed as dimensionless parameters involving surface tension and the partial gas pressures [12]. The initial conditions are:

$$\rho(0) = 1 \tag{11}$$

$$A(0) + F(0) = 1 + \mu \tag{12}$$

$$\frac{F(0)}{A(0) + F(0)} = X_F \tag{13}$$

These efforts represent the continuation of task 1c and the start of task 1e (see original SOW in the Appendix).

Elasticity effects

If we consider the shell to be elastic with shell elasticity E^S and the equilibrium radius to be the initial radius R_o, doing pressure balance [13] we have

$$(C_A + C_F)R_G T = P_A + P_F = \frac{2\sigma}{R} + P_{atm} + \frac{2E^S}{R}\left[\left(\frac{R}{R_o}\right)^2 - 1\right] \tag{14}$$

By defining:

$$\gamma = \frac{2E^S}{P_{atm} R_o} \tag{15}$$

Eqn (14) can be re-written in the following form:

$$F + A = \mu\rho^2 + \rho^3 + \gamma(\rho^4 - \rho^2) \quad (16)$$

Notice that if surface tension is set to zero in equation (10) the minimum value for the ratio R/R_0 is 1. When R/R_0 equals 1, the elasticity term vanishes in Eqn (14) and the inside pressure becomes equal to the atmospheric pressure.

In vitro experiments

A system was built to perform EEI and measure the enhancement of scattered signals from contrast microbubbles in a water bath with three single-element spherically-focused transducers (Staveley, East Hartford, CT, USA), as shown in Figure 1. An excitation transducer (1.1 or 2.1 MHz) with a diameter of 2.5 cm and a focal length of 5.0 cm was used for conditioning microbubbles and a pair of small broadband imaging transducers (with center frequencies of 2-10 MHz), for detecting these microbubbles before and after conditioning. Both imaging transducers had a diameter of 1.2 cm and a focal length around 2.6 cm. The three transducers were placed confocally and the positioning was guided with a 0.2 mm miniature needle hydrophone (Precision Acoustics, Dorchester, UK). The advantage of this measurement system is its high spatial resolution. This is because scattered signals only come from the microbubbles in the small overlapping confocal region of the transmit and receive transducers. The size of the confocal region is determined by the beam diameter (less than 2 mm) at the focus of each transducer.

The excitation transducer was driven by a programmable arbitrary function generator (LW420; LeCroy, Chestnut Ridge, NY, USA) through a 500 W power amplifier (A-500; ENI, Rochester, NY, USA). Unfortunately, this power amplifier broke beyond repair halfway through the project. After 4 months of attempting repairs, we managed to secure funds from other sources to purchase a replacement unit. Getting the purchase order approved took an additional 2 months, before a 3100L power amplifier (ENI, Rochester, NY, USA) was acquired instead. This amplifier covers the frequency range of 125 kHz to 125 MHz providing 50 dB gain for up to 100 W input. Nonetheless the project was delayed by this equipment problem.

The remainder of the setup was, as previously described, based on an imaging transducer, which was used to transmit imaging pulses produced by a programmable function generator (8116A; Hewlett Packard, Santa Clara, CA, USA) and a broadband power amplifier (325LA; ENI) and another transducer, which was employed to receive signals scattered from the contrast microbubbles. The scattered signals were amplified with a low-noise RF amplifier (5052 PR; Parametrics, Waltham, MA, USA) and then acquired using a digital oscilloscope (9350AM; LeCroy, Chestnut Ridge, NY, USA). A time modulus (AV-1023-C; Avtech Electosystems, Ogdensberg, NY, USA) was used to synchronize the delay between the conditioning and imaging pulses. The command delivery to the function generators and the data transfer from the digital oscilloscope were controlled by LabView® (National Instruments, Austin, TX, USA). The acoustic pressure amplitudes were calibrated using a 0.5 mm diameter needle hydrophone (Precision Acoustics Ltd, Dorchester, UK) with an excellent sensitivity over 1 to 20 MHz. This setup represents the completion of Task 1a.

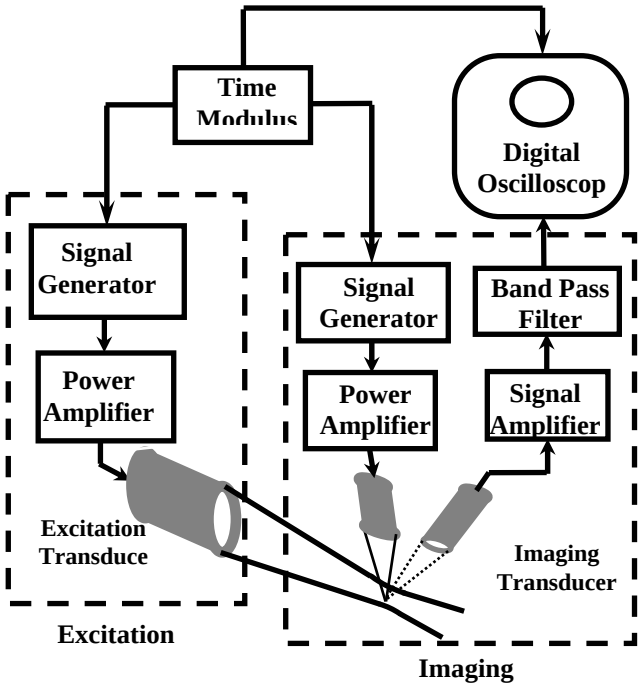

Figure 1. *Experimental set-up for EEI enhancement measurement. An excitation transducer was used to condition contrast microbubbles and a pair of broadband transducers (one for transmission and another for reception, perpendicular to each other and to the excitation transducer) were employed to detect the conditioned microbubbles.*

Six (6) different types of contrast agents were tested: a) Sonazoid® (GE Healthcare, Oslo, Norway), a lipid-coated contrast agent containing a PFC gas (this agent was studied to establish a baseline performance); b) Definity® (Bristol-Myers Squibb Diagnostic Imaging, N Bilerica, MA, USA), a lipid-shelled agent filled with octafluoropropane; c) Optison® (GE Healthcare, Princeton, NJ), an albumin-encapsulated agent filled with perfluorobutane; d) BG1135 (Bracco Research SA, Plan-les-Ouates, Switzerland), an experimental, polymeric shell agent consisting of air-filled microbubbles; e) QFX (Nanfang Hospital, Guangzhou, China), made up of PFC microbubbles stabilized with albumin coating; and f) Therimage (Focus Therapeutics LLC, Media, PA, USA), an experimental, surfactant stabilized agent consisting of air-filled microbubbles. During the experiments, contrast agents were diluted in water and a magnetic stirrer was used to maintain mixture. Concentrations of 1, 10, 20 and 30 μl of contrast agent per liter of water were tested. Excitation amplitudes of 0.4, 0.8, 1.2 and 1.6 MPa were investigated along with excitation pulse lengths of 2 to 35 cycles operating at pulse repetition frequencies (PRFs) of 2, 10 and 20 Hz. Inter-pulse delays from 10 to 750 μs were studied.

In vitro experiments were conducted at ambient temperature (22º C) and physiological temperature (37º C). For each enhancement measurement, spectra of scattered imaging signals from unconditioned and conditioned contrast microbubbles were acquired. The average spectrum for regular contrast microbubbles (before conditioning) was obtained at a given PRF based on a sequence of 64 scattered signals from transmit imaging pulses. The same imaging

pulse was transmitted with a given delay after each condition pulse for 64 times (at the same PRF), so that the averaged spectrum for the conditioned microbubbles was obtained. This represents the continuation of tasks 1d and 1e (see original SOW in the Appendix).

Two different scanning platforms were selected for initial implementation of real-time EEI. One platform was the state-of-the-art, all digital, flagship ultrasound scanner from GE: the Logiq 9 (GE Healthcare, Milwaukee, WI). The second platform selected was an AN2300 digital ultrasound engine (Analogic Corporation, Peabody, MA). This is a development platform featuring a 64 channel digital beamformer front end with continuous dynamic receive focus and apodization, a 40 MHz vector processor, scan converter, real-time controller, and a PC system host with a Windows NT operating system. The AN2300 comes with high level software toolboxes allowing acquisition, analysis and display to be implemented and controlled through ANSI C and C++ routines.

In both scanners the EEI software modifications supported real time and intermittent frame rates operating in fundamental as well as pulse inversion harmonic imaging (HI) grayscale EEI modes. Moreover, EEI was implemented to enable the transmission of an excitation pulse followed by an imaging pulse (or 2 imaging pulses in the case of pulse inversion HI) on a vector-by-vector basis. This transmission mode is similar to standard color Doppler firing modes (albeit with only 2-3 firings along each scan line), which made implementation easier. The standard signal processing chain was then used to produce real time EEI.

Both the Logiq 9 and the AN2300 scanners were successfully modified to incorporate the necessary software changes enabling the transmission of an excitation pulse followed by an imaging pulse (or two for pulse inversion HI) on a vector-by-vector basis (this work was supported in parts by NIH HL62830). Following the modifications, EEI could be performed in fundamental as well as pulse inversion HI grayscale modes at frame rates of either 1 or 30 Hz (i.e., intermittent or real time EEI). As of today we have not identified an endocavitary probe with sufficiently broad bandwidth to accommodate both low frequency excitation pulses and high frequency (> 7 MHz) imaging pulses. Hence, two broad bandwidth transducers, the 3.5C and the P4-2 (Philips Medical Systems, Bothell, WA) were selected for the Logiq 9 and the AN2300, respectively, because of their ability to accommodate the requirements for low frequency excitation pulses (< 3 MHz) and comparable or higher frequency imaging pulses [5]. The excitation pulse employed on the Logiq 9 was a 1.6 MPa, 4 cycle, 2.5 MHz pulse. The AN2300 utilized a longer, lower frequency excitation pulse (12 cycles at 2.0 MHz) to compensate for the lower pulse amplitude of 1.1 MPa. Both scanners were configured to transmit and receive at 2.2 and 4.4 MHz, respectively, in pulse inversion HI mode, while the Logiq 9 operated at 3.6 MHz and the AN2300 at 3.2 MHz in fundamental EEI mode. The delay between the excitation and the imaging pulse was previously found to have limited effect on the enhancement produce in EEI mode [5] and was selected to be 375 μs and 100 μs on the Logiq 9 and the AN2300, respectively. This represents the beginning of task 2c as outlined in the original SOW (see the Appendix).

To demonstrate the contrast imaging enhancement achievable with EEI *in vitro*, a tissue-mimicking flow phantom with an 8 mm vessel embedded (Model 524; ATS laboratories, Bridgeport, CT) was imaged. During the experiments, contrast agents were diluted in water

(e.g., around 20 μl of reconstituted Sonazoid per liter of water) and a magnetic stirrer was used to maintain mixture while the diluted microbubble suspension was pumped through the flow system by a continuous flow roller pump (S10K II; Sarns Inc., Ann Arbor, MI). The amplitude of the excitation pulses was varied from maximum (0 dB) to minimum (-20 dB i.e., no excitation pulse) and EEI was performed in fundamental as well as harmonic mode. Digital cine-clips and images were recorded before and after transmission of the excitation pulses and transferred to a PC for off-line analysis. The mean video intensity in a region of interest (ROI) corresponding to the vessel was determined using Image-Pro Plus software (Media Cybernetics, Silver Spring, MD) and the signal-to-noise-ratio (SNR) relative to baseline (i.e., no excitation pulse) was calculated in dB. The effect of excitation pulse amplitude on the SNR and, thus, on the EEI enhancement, was analyzed statistically and compared using a one-way analysis of variance (ANOVA; Matlab, The Mathworks Inc, Natick, MA) with p-values less than 0.05 considered significant. The SNR was the dependent variable, while amplitude was considered the independent variable. This represents the initiation of tasks 2c and 2d as outlined in the original SOW (see the Appendix) and has been published in a peer-reviewed journal [14].

In vivo experiments

Four laboratory bred mongrel dogs (mean weight: 21 kg and purchased with funds from NIH HL62830) were used for the initial evaluation of *in vivo* EEI. The dogs were pre-medicated with intramuscular administration of a mixture of 0.04 mg/kg atropine sulfate (Anthony Products, Arcadia, CA), and 0.75 mg/kg acepromazine (Promace; Aveco, Fort Dodge, IA). The dogs were placed on a warming blanket to maintain body temperature within normal range. A facemask with Isoflurane 4 to 5 % (Iso-thesia; Abbott Labs, N.Chicago, IL) was used for induction of anesthesia, which was maintained with 0.5 to 2 % of Isoflurane during the entire procedure. An 18 gauge angiocatheter was placed in a forelimb vein in the dogs for contrast material administration. The animal studies were performed under supervision of a veterinarian and fully conformed to the National Institutes of Health guidelines for use of laboratory animals. All protocols were approved by the University's Animal Use and Care Committee.

As an initial test of EEI transcutaneous as well as open chest cardiac imaging was performed using both of the designed scanner configurations. The contrast agents QFX (in 0.5 to 1.5 ml dosages), Sonazoid (in 0.1 to 0.25 ml dosages) and Optison (in 0.5 to 2.0 ml dosages) were evaluated based on the simulation studies and *in vitro* results.

5.2 Results and Discussion

To examine the validity of our novel simulation model, we used the Rayleigh-Plesset equation of Eqn (3) with parameters κ^S = 0.01 msP and γ = 0.6 N/m to simulate the dynamic behavior of microbubbles. The far-field nonlinear scattering was computed from the time evolution of bubble radius using Eqn. (4). After performing an FFT, the subharmonic response was compared to experimental observations (for details on the experimental data acquisition see [15]). The simulation is scaled to match the experimental data for the lowest pressure level. Note that the model parameters were determined using the linearized equations valid only for small oscillations. The underlying assumption is that a Newtonian rheology holds for the interface, and the determined material properties remain constant in a range of magnitude of

oscillation (they may change for too large an oscillation, e.g. shear rate dependent interface viscosity and interfacial tension).

Figure 2 shows subharmonic emission for Sonazoid at several frequencies along with the model prediction. For comparison, the predictions from Church-Hoff model have also been included. The corresponding root-mean-square-error (RMSE) for the estimation using the two models is presented in Table 1. At frequencies of 3 and 4.4 MHz, the new model predicts better than the Church-Hoff model, whereas at frequencies of 2 and 6 MHz, the performance of two models are comparable with the Church-Hoff model performing slightly better. These results were published in a peer-reviewed journal [7].

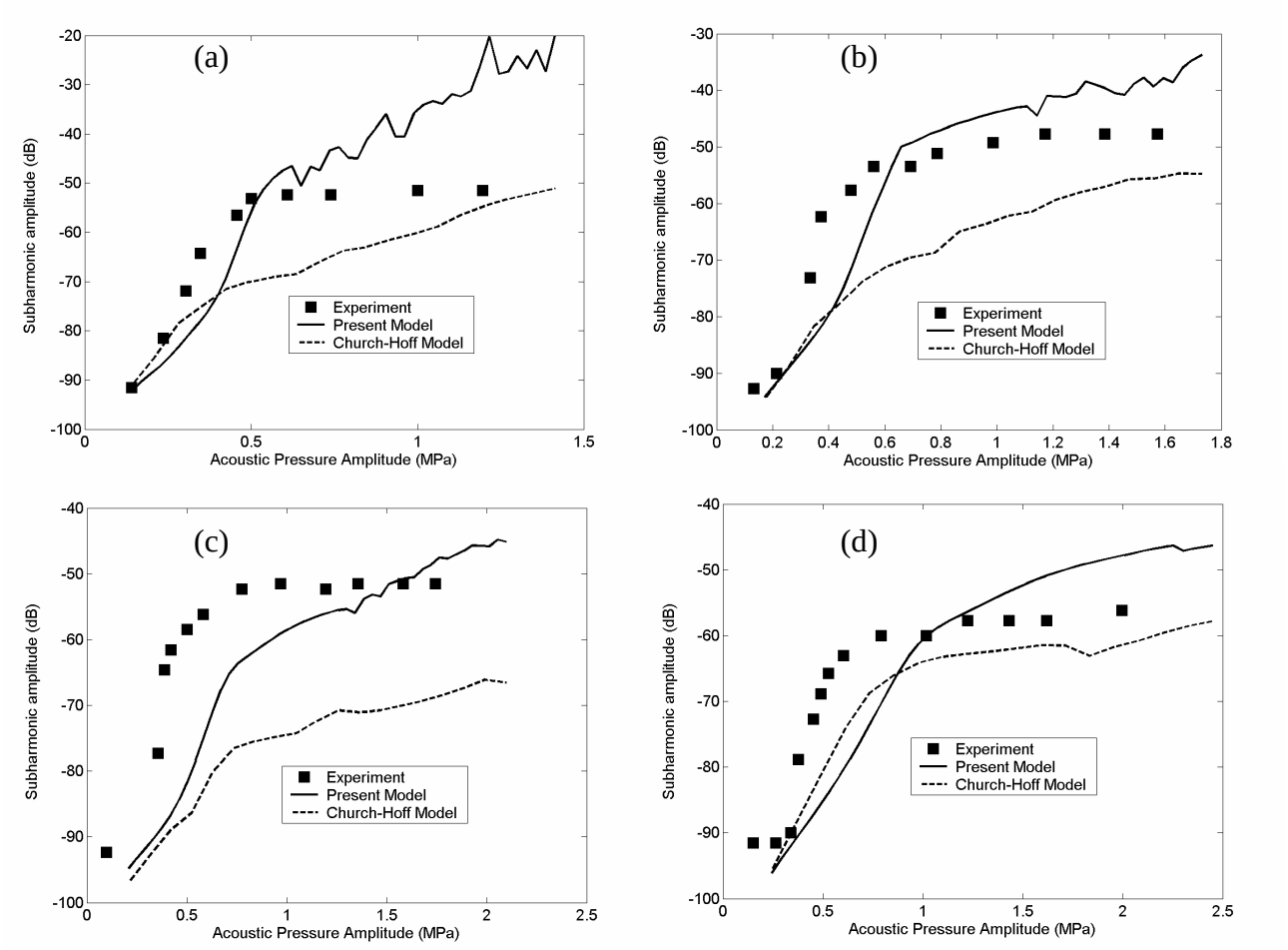

Figure 2. *Predicted and measured subharmonic response at various acoustic pressure amplitudes for Sonazoid. Center frequencies used in these results are as follows: (a) 2.0 MHz, (b) 3.0 MHz, (c) 4.4 MHz and (d) 6.0 MHz.*

Table 1: Error in estimating the subharmonic response of Sonazoid using the new model and the Church-Hoff model.

Driving frequency (MHz)	RMSE (%)	
	New Model	Church-Hoff Model
2.0	22.42	19.69
3.0	16.62	26.08
4.4	24.91	40.36
6.0	16.36	12.10

The ability of our novel simulation model [7] to simulate the dynamic behavior of microbubbles during EEI was examined (using parameters κ^s = 0.01 msP and γ = 0.6 N/m). The excitation and imaging pulses used are depicted in Figure 3 (for two different inter-pulse delays). At an imaging frequency of 3 MHz the model was not able to reproduce the experimental results and did not show an effect due to the excitation field. Moreover, for the short inter-pulse delay of 10 μs the model simply adds the response of the excitation and the imaging pulses, which does not correspond to the experimental results obtained *in vitro* [5, 14]. However, there was a small enhancement of 4 dB when the imaging frequency was increased to 7.5 MHz (for a delay of 100 μs), which appear to be caused by ringing effects produced by the excitation pulse. Consequently, it was decided to attempt to produce a more realistically bubble simulation model by incorporating bubble growth via rectified diffusion.

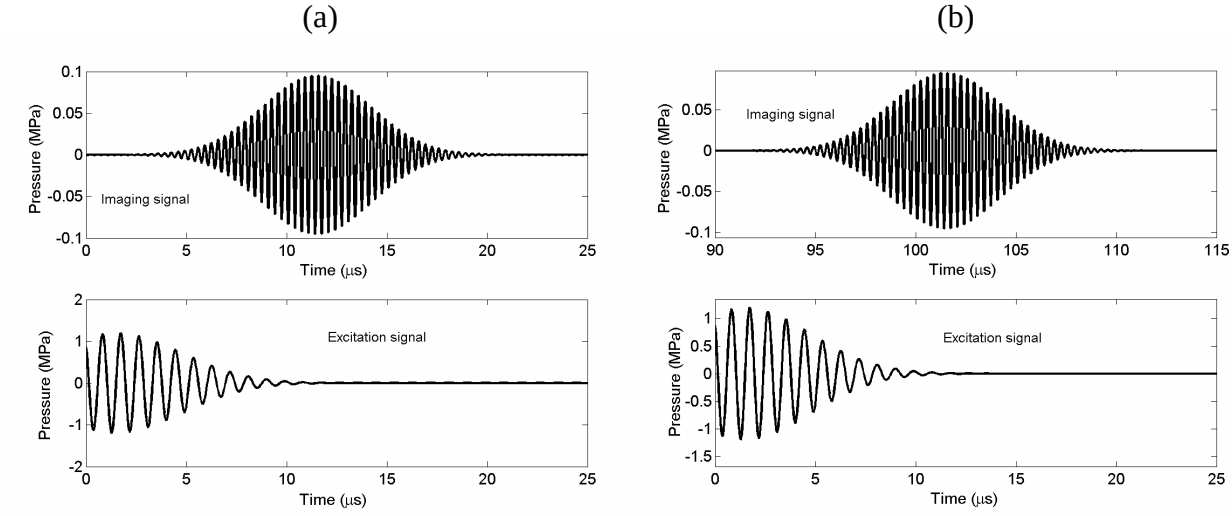

Figure 3. *Simulated excitation and imaging pulses for EEI with Sonazoid. The inter-pulse delays were (a) 10 μs and (b) 100 μs.*

The new model of bubble growth and dissolution was implemented in Matlab (The Mathworks, Natick, MA). The variation of the R/R_o with time for varying X_F (where $X_F = 1$ indicates no air and $X_F = 0$ indicates no fluorocarbon inside the bubble) is shown in the Figure 4. The outside medium is saturated with air void of the perfluorocarbon. As the mole fraction of the osmotic agent (fluorocarbon) goes on increasing the growth gets bigger and the dissolution time keeps on increasing [14]. This causes initial bubble growth due to the sudden ingression of the air into the bubble [16], since the coefficient of diffusivity of the air is higher than that of perfluorocarbon.

Figure 5 shows the change in R/R_o as a function of time for bubbles with no shell, a permeable and a less permeable shell ($X_F = 1$). As the permeability of the shell decreases the life time of the bubble increases from around 10 seconds for the free bubble to couple of minutes for a bubble with a less permeable shell. The free bubble (i.e., without a shell) can be considered a case of a shell with infinite permeability. The thickness of the shell can be increased to reduce the permeability (inversely proportional to shell thickness) and, hence, increase the life time of a bubble.

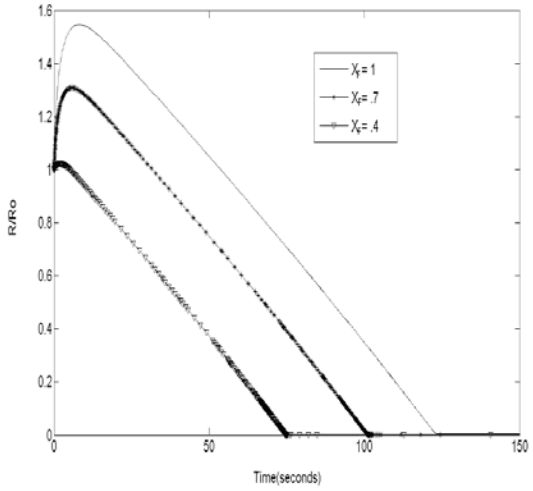

Figure 4. *The variation in R/R_o with time for varying mole fractions of perfluorocarbon assuming a permeable shell and $f = 1$.*

Figure 5. *Changes in R/R_0 over time for different shell types.*

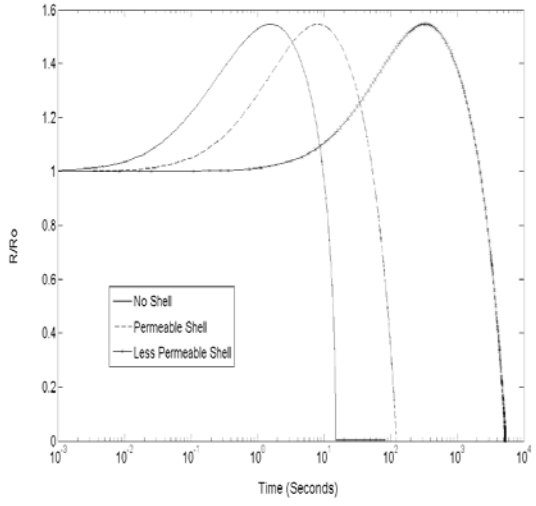

The effect of the elasticity term introduced in Eqn (14) is demonstrated in Figure 6. When the elasticity is reduced by a factor 100 the bubble grows by 2.2 times even though there is no extra pressure inside the bubble to drive the gases out of the bubble. Notice that R/R_o does not achieve values below 1 as there is no σ to make inside pressure higher.

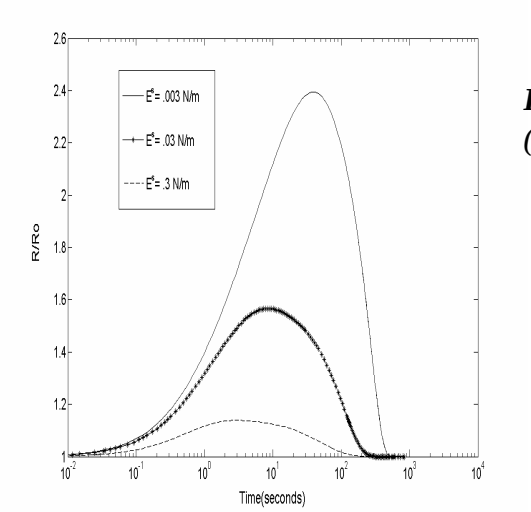

Figure 6. *R/R_0 plotted over time for varying E^S values (using a permeable shell and σ = 0 N/m).*

In contrast Figure 7 shows R/R_0 for the same elasticity parameter and an σ of *0.7* N/m, which allows the inside pressure to be still higher than the outside pressure for R/R_0 of 1. However, if R/R_0 is less than 1 in Eqn (14) the elasticity term becomes negative and acts towards decreasing the pressure inside the bubble. Nonetheless the surface tension term will drive the gas out of the bubble provided it dominates the elasticity parameter. If the elasticity term dominates the surface tension term then the bubble will not dissolve as can be seen for the case E^s =.3 N/m in Figure 7. Hence, the elasticity term competes with the surface tension term and plays a vital role in the growth as well as dissolution of the bubble, which is an important new observation that our model has provided. The ability of our simulation model to simulate the dynamic behavior of Sonazoid microbubbles during EEI was also examined as shown in Figure 8. At an imaging frequency of 7.5 MHz the model reproduced the experimental results to some degree showing 20 and 35 dB enhancement at the fundamental and the harmonic frequencies, respectively, due to the excitation field. However, this is much higher values of enhancement than measured experimentally and enhancement is also seen at other frequencies than at 7.5 and 15 MHz. Efforts are ongoing to produce a more realistic model.

Examples of *in vitro* images recorded in the cine loop of the Logiq 9 scanner before and after transmission of the excitation pulse at a 1 Hz frame rate (i.e., intermittent EEI) are given in Figure 9. Conventional pulse inversion HI of the phantom vessel containing BG1135 in Figure 9a shows the vessel poorly, because the contrast echoes are *en par* with the tissue echoes. Following application of the excitation pulse, a marked enhancement in contrast signals within the vessel, but a minimal enhancement in tissue echoes, is observed (Figure 9b). Similar results were obtained with Sonazoid and QFX. The change in SNR obtained with EEI relative to standard contrast imaging was measured as a function of excitation pulse amplitude.

Figure 7. *R/R_0 plotted over time for varying E^S values (using a permeable shell, $\sigma = 0.7$ N/m and $f = 1$)*

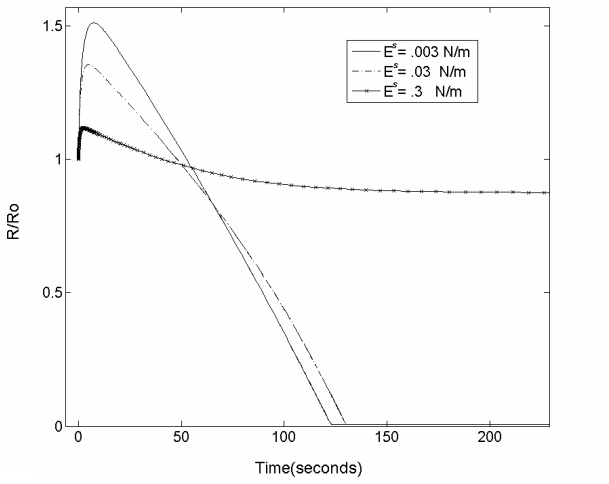

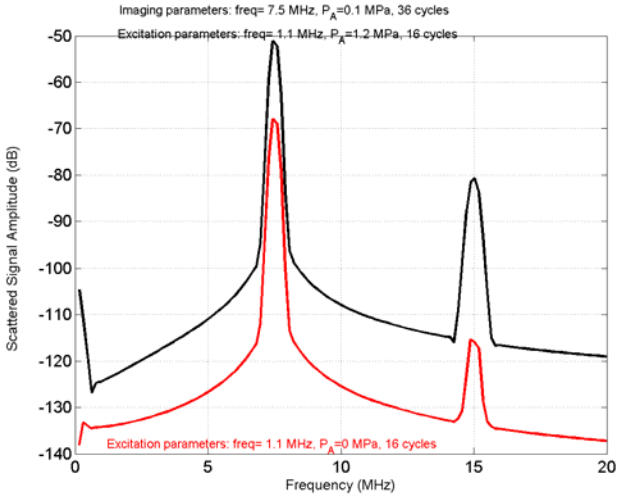

Figure 8. *Simulation of enhancement from Sonazoid in EEI mode using 1.1 MHz excitation at 1.2 MPa, imaging at 7.5 MHz. More than 20 dB enhancement occurs at the fundamental and the harmonic frequency.*

(a) (b)

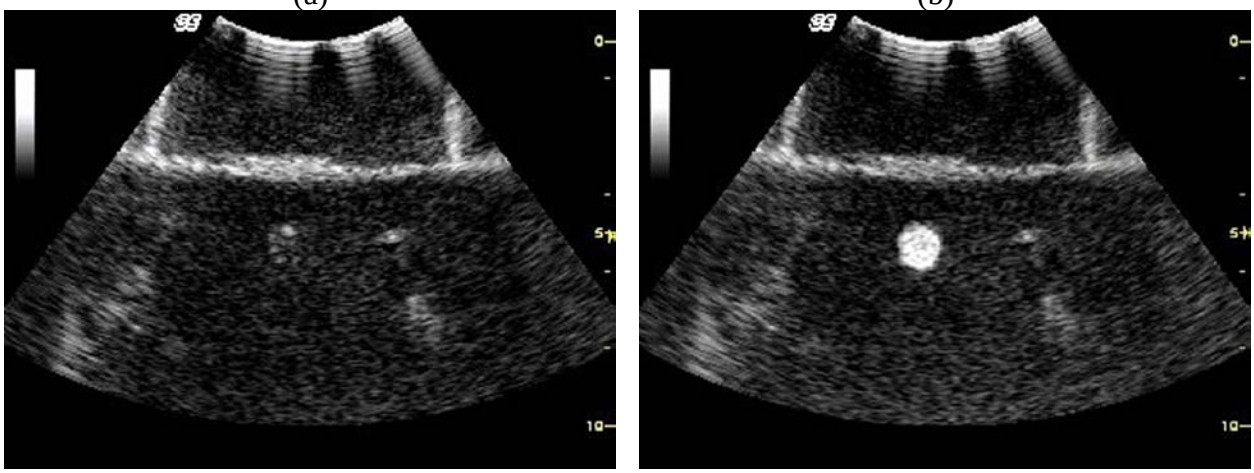

Figure 9. *Intermittent, pulse inversion HI of BG1135 obtained with the Logiq 9 scanner (a) without EEI and (b) with EEI. Notice the marked improvement in SNR within the vessel following activation of EEI.*

In Figure 10, an example based on measurements with the contrast agent BG1135 imaged in HI mode is shown. The maximum improvement in SNR was 10.4 dB. On average the improvement was 6.3 dB ± 1.29 dB, which was measured for a -4 dB excitation pulse amplitude (cf., Figure 10). The ANOVA showed the effect of EEI was significant ($p = 0.0007$). In fundamental mode the best SNR measured with QFX was 7.8 dB, while the mean improvement in SNR was found to be 4.1 dB ± 0.13 dB for a -6 dB excitation amplitude ($p < 0.0001$). These SNR improvements are somewhat lower (by 4 – 6 dB) than those measured with the EEI pulse-echo set up [5]. Most likely this is caused by the flow of conditioned microbubbles out of the imaging plane and the differences in transducer sensitivity that occur when single element transducers are replaced by broad bandwidth arrays. Moreover, the slightly reduced enhancement observed at the highest excitation amplitudes in Figure 10 is probably due to bubble destruction i.e., destroyed microbubbles were not completely replenished between excitation pulses. Thus tasks 2c and 2d as outlined in the original SOW (see the Appendix) have been initiated.

Unfortunately, BG1135 is an experimental agent (manufactured by Bracco) and it cannot currently be made in a sterile form, which precludes its use for *in vivo* applications. Hence the initial *in vivo* assessments were conducted using the contrast agents Sonazoid and QFX. Examples of the former agent imaged in fundamental EEI mode and the latter in harmonic EEI mode are shown in Figure 11. There is very little to no enhancement seen in the ventricles when the activation pulse initiating EEI was employed. This was obviously a rather disappointing *in vivo* result and it was, therefore decided to conduct further *in vitro* investigations to improve our understanding of the phenomena behind EEI.

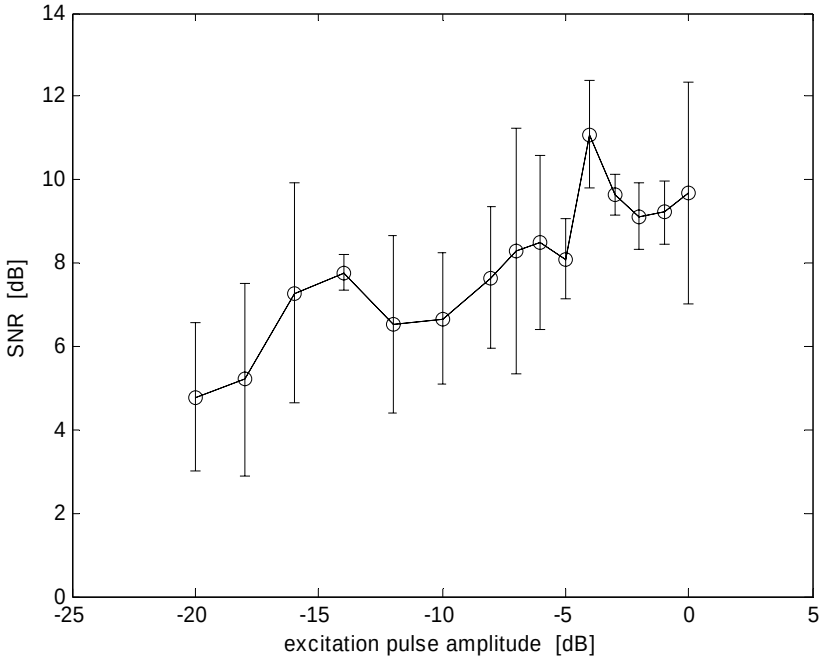

Figure 10. *Changes in SNR as a function of excitation amplitude for BG1135 imaged in HI mode. The -20 dB amplitude corresponds to conventional HI (i.e., baseline without EEI).*

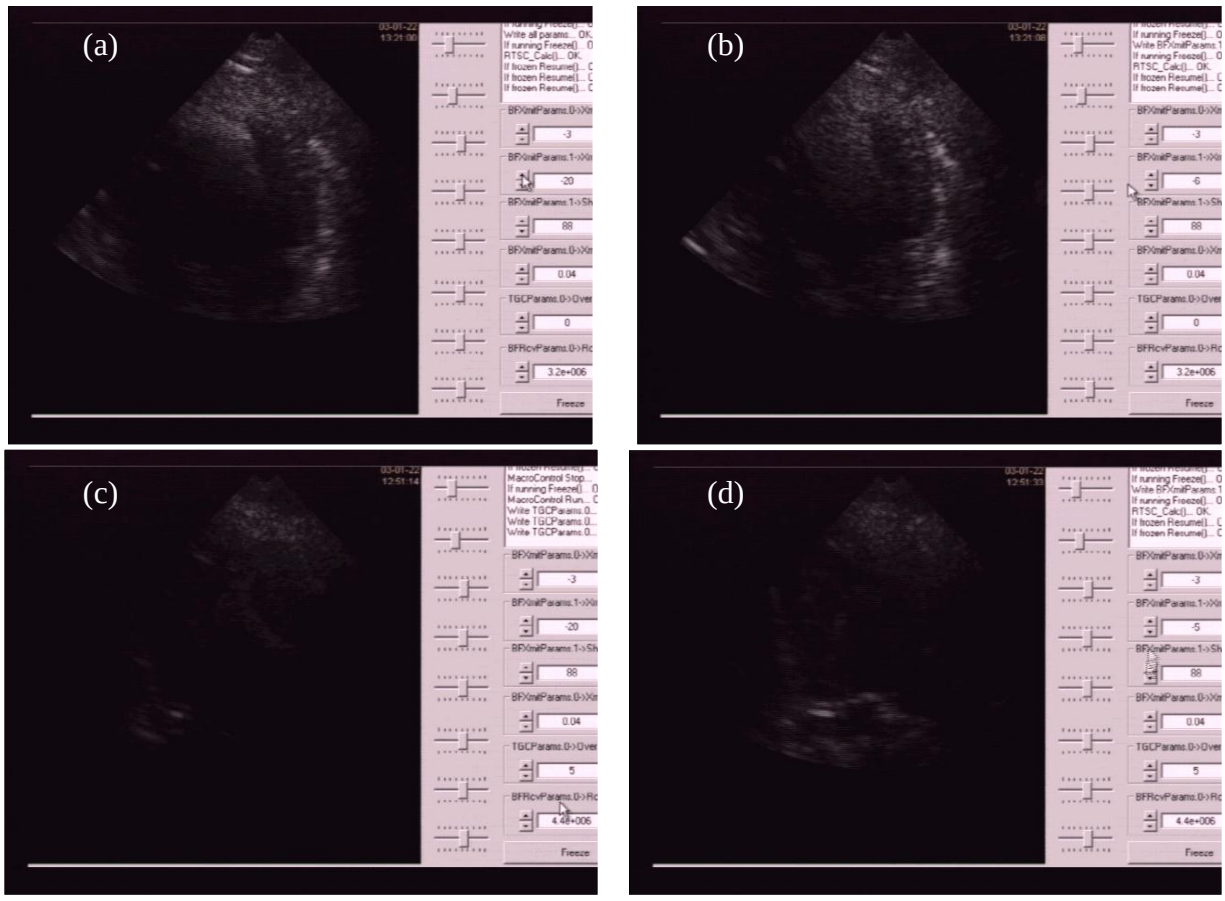

Figure 11. *Examples of in vivo cardiac EEI obtained with the AN2300 in a canine model. Sonazoid imaged in fundamental mode (a) without and (b) with EEI; QFX imaged in HI mode (c) without and (d) with EEI. No discernible difference in enhancement is apparent with the application of EEI.*

A pulse-echo system was built (as outlined in Fig. 1) to perform EEI. The change in scattered signal strength before and after the excitation pulse (i.e., the enhancement obtained with EEI relative to standard contrast imaging) was measured under different acoustic conditions. In Figure 12a, an example based on measurements with Sonazoid at 22° C is shown. EEI induces scattering enhancement with a maximum of approximately 10 dB around 3.0 and 6.0 MHz (the fundamental and second harmonic frequencies) for Sonazoid microbubbles conditioned with 1.2 MPa excitation pulses (1.1 MHz and 16 cycles) at 2 Hz PRF. Imaging pulses (36 cycles, 3.0 MHz and 0.1 MPa) were transmitted, with a delay of 100 μs between the conditioning pulse and the detection pulse. However, when the temperature was elevated to the physiological level (i.e., 37° C; Fig. 12b) no enhancement could be observed. Clearly, this means that EEI with Sonazoid would not be beneficial *in vivo* at physiological temperatures. Similar results were obtained with Definity and QFX, which certainly explains the disappointing results of Figure 11.

(a)

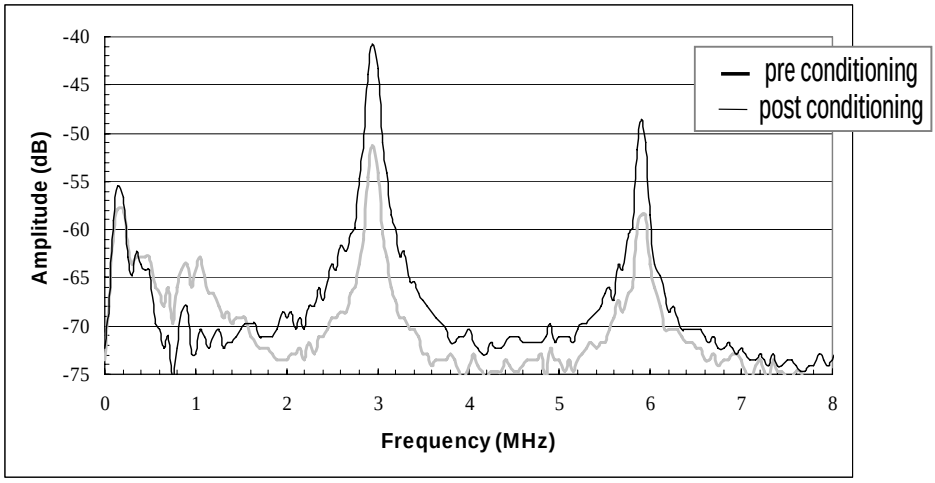

(b)

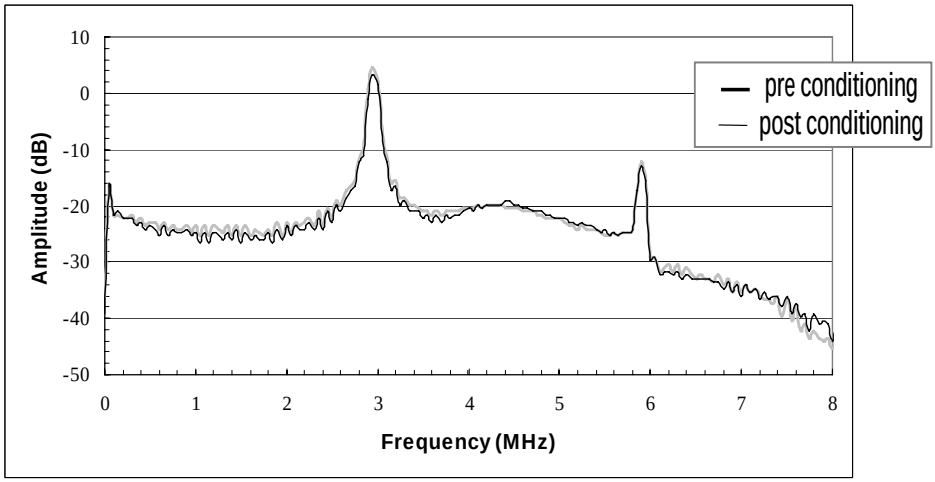

Figure 12. *Measurement of enhancement from Sonazoid in EEI mode using 1.1 MHz excitation at 1.2 MPa, 2 Hz PRF obtained at (a) 22° C and (b) at 37° C. Notice, that no enhancement is seen at the physiological temperature (whereas marked enhancement ~10 dB occurs at room temperature).*

However, EEI with Optison (employing the same conditioning and imaging conditions) produced very different results. Figure 13 demonstrates limited enhancement at 22° C, whereas 10 dB of enhancement is seen at 37° C (Fig. 13b); albeit only at the fundamental frequency (of 3.0 MHz). In Figure 14a, an example based on measurements obtained at 7.5 MHz (i.e. a realistic imaging frequency for the prostate) with Sonazoid at 22° C is shown. EEI induces scattering enhancement with a maximum of approximately 6 dB around 7.5 and 15 MHz (the fundamental and second harmonic frequencies) for Sonazoid microbubbles conditioned with 1.2 MPa excitation pulses (1.1 MHz and 16 cycles) at 2 Hz PRF. Imaging pulses (36 cycles, 7.5 MHz and 0.1 MPa) were transmitted, with a delay of 100 μs between the conditioning pulse and

the detection pulse. However, when the temperature was elevated to the physiological level (i.e., 37° C; Fig. 14b) enhancement reduced to around 3 dB. EEI with Optison (employing the same conditioning and imaging conditions) produced very different results. Figure 15 demonstrates almost the same enhancement at 22° C as at 37° C (approximately 7 and 3 dB at the fundamental and second harmonic frequencies, respectively). These results are very different from the ones obtained with an imaging frequency of 3 MHz (cf. Fig. 13), where Optison produced almost no enhancement at room temperature but almost 10 dB at 37° C. Clearly both temperature and imaging frequency are important parameters for EEI, but the impact varies markedly depending on the particular contrast agent.

(a)

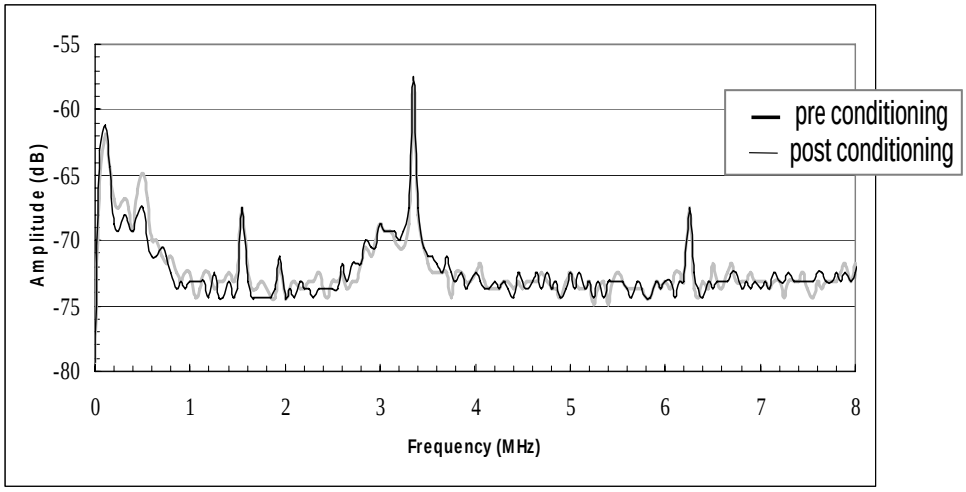

(b)

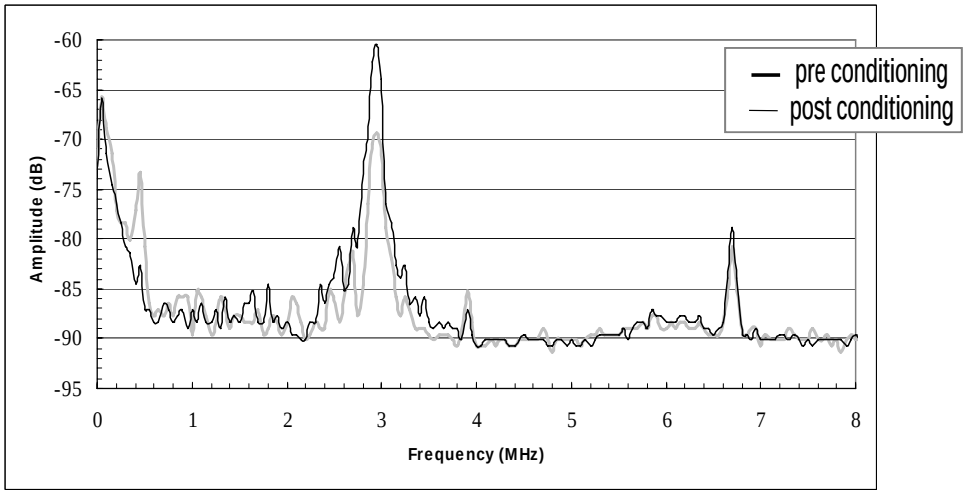

Figure 13. *Measurement of enhancement from Optison in EEI mode using 1.1 MHz excitation at 1.2 MPa, 2 Hz PRF obtained at (a) 22° C and (b) at 37° C. Notice, that no enhancement is seen at room temperature, but at the physiological temperature 10 dB of enhancement is observed at the fundamental frequency.*

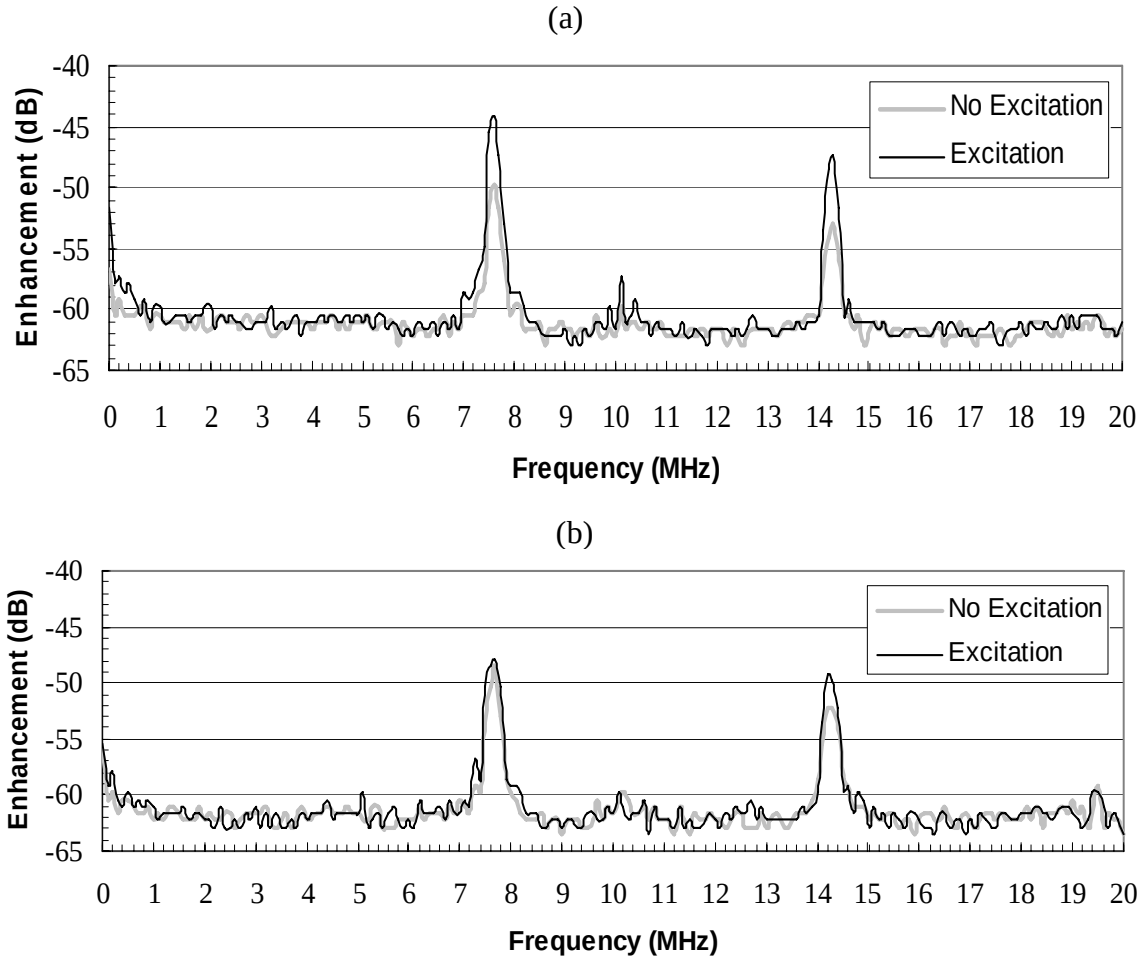

Figure 14. *Measurement of enhancement from Sonazoid in EEI mode using 1.1 MHz excitation at 1.2 MPa, imaging at 7.5 MHz, 2 Hz PRF obtained at (a) 22°C and (b) at 37°C. Notice, that no enhancement is seen at the physiological temperature (whereas marked enhancement ~6 dB occurs at room temperature).*

Nonetheless, these results indicate that *in vivo* fundamental EEI with Optison should be a feasible prospect. Hence, we decided to conduct another canine cardiac imaging experiment (closed as well as open chest; as before). The same experimental conditions as described on page 11 were employed. In Figure 16 the outcome of employing EEI with Optison in fundamental mode is depicted. The 4-chamber view of the heart shows no observable increase in enhancement when using EEI (compare Figs 16a and b), which was obviously a disappointment. Subsequently, the variation in enhancement achievable *in vitro* with Optison was measured (at the physiological temperature of 37° C). Enhancement varied considerably with concentration as demonstrated in Figure 17. More importantly the dose which produced maximum enhancement *in vitro* (0.05 μl/l) was several orders of magnitude lower that the *in vivo* dosages used (on the order of ml's per l). Finally, the *in vitro* enhancement drops off markedly as the dose is changed from the maximum dose (cf., Fig 17). The *in vitro* results are summarized in Table 2.

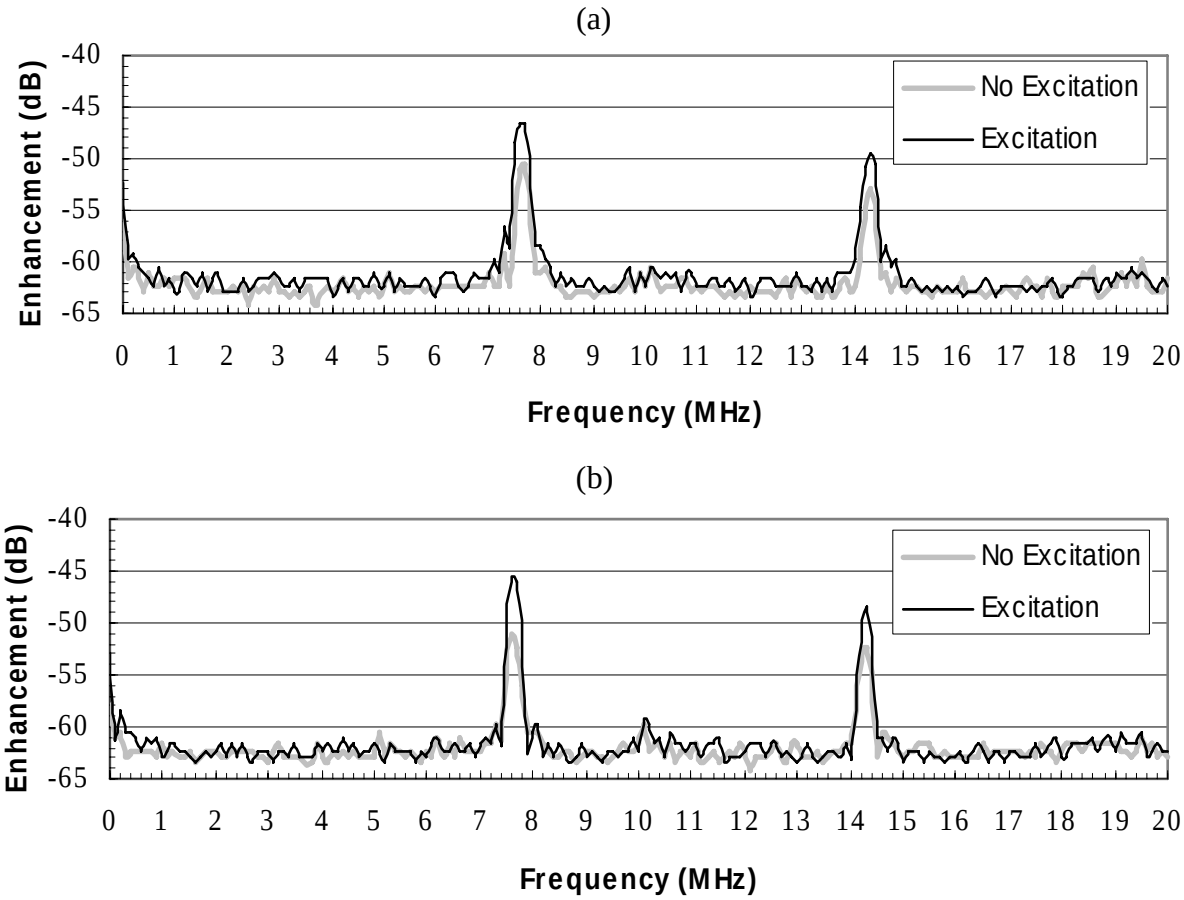

Figure 15. *Measurement of enhancement from Optison in EEI mode using 1.1 MHz excitation at 1.2 MPa, imaging at 7.5 MHz, 2 Hz PRF obtained at (a) 22° C and (b) at 37° C. Notice, that almost the same enhancement is seen at room temperature as at the physiological temperature.*

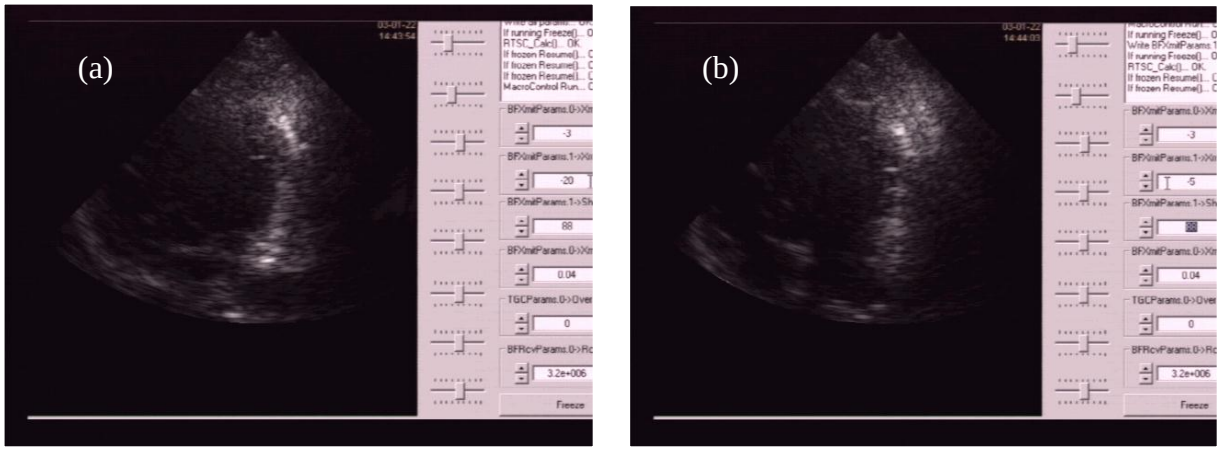

Figure 16. *Example of in vivo cardiac EEI obtained with the AN2300 in a canine model. Optison imaged in fundamental mode (a) without and (b) with EEI. No discernible difference in enhancement is apparent with the application of EEI.*

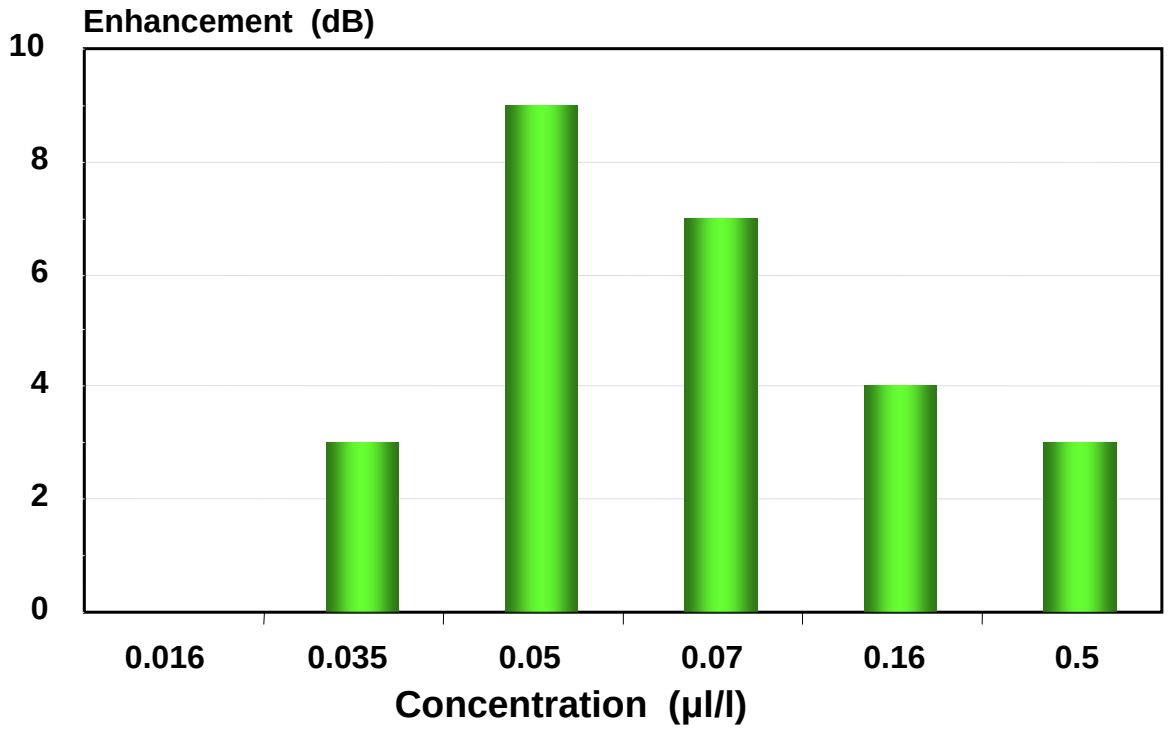

Figure 17. *In vitro measurement of EEI enhancement obtained from Optison as a function of contrast concentration at 37° C. Notice, that maximum enhancement ~9 dB occurs at 0.05 µl/l.*

Table 2: Summary of the *in vitro* measurements as a function of concentration and temperature.

Agent	Concentration (µl/l)	Temperature (° C)	Enhancement (dB)
Sonazoid	20	22	10
		37	1
	45	37	5
Optison	0.05	22	1
		37	10
Definity	30	22	0
		37	0
Therimage	20	22	6
		37	0
QFX	25	22	6
		37	0

6. KEY RESEARCH ACCOMPLISHMENTS

- A dual-transducer pulse-echo system was built to perform EEI.
- A new zero-thickness interface model was developed to describe the encapsulation of microbubble contrast agents.

- Model predictions were compared with measured nonlinear subharmonic signals (even though the model was fitted using linearized dynamics).
- The new zero-thickness interface model was expanded to describe the dual pulse mode of EEI, but further work is necessary.
- The growth and dissolution of microbubbles was also simulated and the shell elasticity identified as playing a vital role in these processes.
- *In vitro* experiments were conducted with 6 contrast agents.
- Temperature and concentration dependencies were studied.
- Initial experiments were conducted at 3.0 and 7.5 MHz with 3 contrast agents.
- Up to 10 dB of enhancement was measured at 37° C for 0.05 μl/l of Optison.
- Both temperature and imaging frequency are important parameters for EEI, but the impact varies markedly depending on the particular contrast agent.
- An initial version of EEI software was implemented on two ultrasound scanners.
- *In vitro* flow phantom measurements with 3 contrast agents demonstrated maximum enhancement of 10.4 dB in harmonic mode (mean enhancement: 6.3 dB; $p = 0.0007$)
- The preliminary *in vivo* experiments were conducted in 4 dogs.
- *In vivo* EEI cardiac imaging - disappointingly - demonstrated no visible enhancement.

7. REPORTABLE OUTCOMES

Peer-Reviewed Journal Articles

K. Sarkar, W. T. Shi, D. Chatterjee, F. Forsberg. Characterization of ultrasound contrast microbubbles using in vitro experiments and viscous and viscoelastic interface models for encapsulation. *J Acoust Soc Am,* vol. 118, vol 118, no. 1, pp. 539-550, 2005.

F. Forsberg, W. T. Shi, M. M. Knauer, A. L. Hall, C. Vecchio, R. Bernardi. Real time excitation enhanced ultrasound contrast imaging. *Ultrasonic Imaging*, vol. 27, no. 2, pp. 65-74, 2005.

Abstracts and Proceedings

F Forsberg, WT Shi, M Knauer, C Vecchio, R Bernardi, BB Goldberg. Real time excitation enhanced ultrasound contrast imaging. *Ultrasound Med Biol*, vol. 29, pp. S96-S97, 2003.

WT Shi, Y Liu, Z Lu, F Forsberg, D Zha, JB Liu, BB Goldberg. Nonlinear imaging with a new contrast agent. *Ultrasound Med Biol*, vol. 29, pp. S97, 2003.

R. J. Ro, F. Forsberg, M. Knauer, W. T. Shi, P. A. Lewin, R. Bernardi. On the temperature and concentration dependency of excitation-enhanced imaging. *Proc Biomed Eng Soc Ann Fall Meetg*, abstract no. 1059, 2004.

P. Jain, K. Sarkar. Growth and dissolution of encapsulated microbubbles used in ultrasound contrast imaging. *Proc. 2006 ASME Joint U.S.-European Fluids Engineering Summer Conference*, FEDSM2006-98550, 2006.

F. Forsberg, R. J. Ro, W. T. Shi, M. K. Knauer, K. Sarkar, A. L. Hall, C. Vecchio, R. Bernardi. Excitation Enhanced Imaging: *in vitro* and *in vivo* results. *Ultrasonic Imaging*, vol. 29, pp. 65-66, 2007.

K. Sarkar, P. Jain. Growth and dissolution of encapsulated microbubbles used for contrast imaging and drug delivery. Accepted for publication in *Proc 6th Int Conf on Multiphase Flows*, 2007.

F. Forsberg, R. J. Ro, W. T. Shi, M. K. Knauer, K. Sarkar, A. L. Hall, C. Vecchio, R. Bernardi. Excitation Enhanced Imaging for prostate cancer detection: *in vitro* and *in vivo* results. Accepted for publication in *Proc. IMPaCT*, 2007.

Presentations

June 1 - 4, 2003	The 47th Annual Convention of the American Institute of Ultrasound in Medicine, and the 10th Congress of the World Federation for Ultrasound in Medicine and Biology, Montreal, Canada. • Real time excitation enhanced ultrasound contrast imaging. • Nonlinear imaging with a new contrast agent
February 6 - 7, 2004	9th Ultrasound Contrast Research Symposium in Radiology, San Diego, CA, USA. • On the temperature and concentration dependency of Excitation-Enhanced Imaging.
October 13-16, 2004	Biomedical Engineering Society Annual Fall Meeting, Philadelphia, PA, USA. • On the temperature and concentration dependency of Excitation-Enhanced Imaging.
July 17 – 20, 2006	2nd ASME Joint U.S.-European Fluids Engineering Summer Meeting, Miami, FL, USA. • Growth and dissolution of encapsulated microbubbles used in ultrasound contrast imaging.
May 16 – 18, 2007	Thirty-Second International Symp. on Ultrasonic Imaging and Tissue Characterization, Washington DC, USA. • Excitation Enhanced Imaging: *in vitro* and *in vivo* results.

8. CONCLUSIONS

A new zero-thickness interface model was developed to describe the encapsulation of microbubble contrast agents. While the model was fitted based on linear measurements, the model predictions were compared to measured nonlinear subharmonic signals. The current model shows a much better match with the experimental data at frequencies of 3.0 and 4.4 MHz than other models. The model was used to simulate the dual pulse imaging mode associated with

EEI. While results at an imaging frequency of 7.5 MHz were somewhat in agreement with measurements, the enhancement was unrealistically high (20-35 dB). Further work is ongoing to improve upon the model by incorporating the growth and dissolution of microbubbles. Initial simulation results indicate that the shell elasticity plays a vital role in the growth as well as dissolution of the bubbles.

A pulse-echo system was built to perform in vitro EEI measurements and experiments were conducted with 6 contrast agents. Up to 10 dB of enhancement was measured at 37° C with Optison. The pulse-echo system was used to perform *in vitro* EEI measurements at 7.5 MHz and initial experiments were conducted with 3 contrast agents. From 6 to 10 dB of enhancement was measured with Optison irrespective of temperature, whereas Sonazoid produced 6 dB of enhancement at 22° C and only 3 dB at 37° C. Enhancement varied considerably with concentration as demonstrated in Figure 17. More importantly the dose which produced maximum enhancement *in vitro* (0.05 μl/l) was several orders of magnitude lower that the *in vivo* dosages used (on the order of ml's per l). Finally, the *in vitro* enhancement drops off markedly as the dose is changed from the maximum dose.

Finally, a Logiq 9 scanner with a 3.5C curved linear array and an AN2300 digital ultrasound engine with a P4-2 phased array transducer were modified to perform EEI on a vector-by-vector basis in fundamental and pulse inversion harmonic grayscale modes. Ultrasound contrast microbubbles within an 8 mm vessel embedded in a tissue-mimicking flow phantom were imaged *in vitro*. While video intensities of scattered signals from the surrounding tissue were unchanged, video intensities of echoes from contrast bubbles within the vessel were markedly enhanced. The maximum enhancement achieved was 10.4 dB in harmonic mode (mean enhancement: 6.3 dB; $p = 0.0007$).

Preliminary *in vivo* fundamental and harmonic EEI was conducted with 3 contrast agents in a cardiac application (partially funded by the NIH). The *in vivo* results showed no observable increase in enhancement when using EEI, which was obviously a disappointment. However, EEI appears to be quite sensitive to changes in temperature and microbubble concentration, which may explain the reduced enhancement observed *in vivo*. Further research is needed to clarify this issue.

In summary, task 1 has been completed while task 2 has been partially completed. Initial *in vivo* EEI imaging has been conducted (as envisaged under Task 3), but in a different animal model.

9. REFERENCES

1. Halpern EJ, Frauscher F, Forsberg F, Nazarian LN, O'Kane P, Gomella LG. High-frequency Doppler US of the prostate: effect of patient position. *Radiology,* 222:634-639, 2002.
2. Pryor MB, Schellhammer PF. The pursuit of prostate cancer in patients with a rising prostate-specific antigen and multiple negative transrectal ultrasound-guided prostate biopsies. *Clin Prostate Cancer*, 1:172-176, 2002.
3. Goldberg BB, Raichlen JS, Forsberg F. *Ultrasound Contrast Agents: Basic Principles and Clinical Applications* (2nd Ed). Martin Dunitz Ltd., England, 2001.
4. de Jong N, Cornet R, Lancee CT. Higher harmonics of vibrating gas-filled microspheres. part one: simulations. *Ultrasonics*, 32:447-453, 1994.
5. Shi WT, Forsberg F, Bautista R, Vecchio C, Bernardi R, Goldberg BB. Image enhancement by acoustic conditioning of ultrasound contrast agents. *Ultrasound Med Biol*, 30:191 – 198, 2004.
6. Chatterjee D, Sarkar K. A Newtonian rheological model for the interface of microbubble contrast agents. *Ultrasound Med Biol*, 29:1749-1757, 2003.
7. Sarkar K, Shi WT, Chatterjee D, Forsberg F. Characterization of ultrasound contrast microbubbles using in vitro experiments and viscous and viscoelastic interface models for encapsulation. *J Acoust Soc Am*, 118: 539-550, 2005.
8. Brennen CE. *Cavitation and Bubble Dynamics*. Oxford University Press, New York, 1995.
9. Church CC. The effects of an elastic solid surface layer on the radial pulsations of gas bubbles. *J. Acoust. Soc. Am.*, 97:1510-1521, 1995.
10. Hoff L, Sontum PC, Hovem JM. Oscillations of polymeric microbubbles: effect of the encapsulating shell. *J. Acoust. Soc. Am.*, 107:2272-2280, 2000.
11. Hoff L. *Acoustic characterization of contrast agents for medical ultrasound imaging*. Ph.D. thesis, Norwegian University of Science and Technology, 2000.
12. P. Jain, K. Sarkar. Growth and dissolution of encapsulated microbubbles used in ultrasound contrast imaging. *Proc. 2006 ASME Joint U.S.-European Fluids Engineering Summer Conference*, FEDSM2006-98550, 2006.
13. Chatterjee D, Jain P, Sarkar K. Ultrasound–mediated destruction of contrast microbubbles used for medical imaging and drug delivery. *Phys. Fluids*, 17:100603 – 100603-8, 2005.
14. Forsberg F, Shi WT, Knauer MM, Hall AL, Vecchio C, Bernardi R. Real time excitation enhanced ultrasound contrast imaging. *Ultrasonic Imaging*, 27: 65-74, 2005.
15. Shi WT, Hoff L, Forsberg F. Subharmonic performance of contrast microbubbles: an experimental and numerical investigation. *Proc IEEE US Symp*, 1908-1911, 2002.
16. Kabalnov A, Klein D, Pelura T, Schutt E, Weers J. Dissolution of multicomponent microbubbles in the blood stream: 1. Theory. *Ultrasound Med. Biol.*, 24: 739-749, 1998.
17. Forsberg F, Basude R, Liu JB, Alessandro J, Shi WT, Rawool NM, Goldberg BB, Wheatley MA. Effect of filling gasses on the backscatter from contrast microbubbles: theory and *in vivo* measurements. *Ultrasound Med. Biol.*, 25: 1203 - 1211, 1999.

Appendix I

The Statement of Work from the original proposal:

Task 1: To investigate activation-induced scattering enhancement at different center frequencies, amplitudes, and shapes (or lengths) of activation pulse sequences (Months 1-18):

a. Construct an *in vitro* experimental system for ultrasonically activating contrast microbubbles and measuring the resulting changes in backscattering (Months 1-2).
b. Design and develop numerical codes for a theoretical model describing the dynamics and instability of ultrasonically activated contrast microbubbles (Months 1-6).
c. Calculate the behavior of individual contrast microbubble and the collective behavior of contrast microbubble populations (Months 6-18).
d. Measure changes in backscattered fundamental, second and sub-harmonic signals before and after activation (Months 3-18).
e. Predict optimal contrast agents for ultrasound-activated contrast imaging accordingto the numerical simulations (Months 12-18)
f. Select optimal contrast agents for ultrasound-activated contrast imaging. The selection is mainly based on experimental measurements (Months 12-18).
g. Develop activation and imaging strategies, based on both numerical simulations and experimental measurements for the scattering enhancement (Months 12-18).

Task 2: To implement ultrasound-activated contrast imaging (Months 18-24):

a. Produce and evaluate activation-enhanced A-lines in an *in vitro* perfusion phantom using the simple pulse-echo system (Months 18-20).
b. Optimize activation and imaging strategies, based on *in vitro* phantom measurements and simulations with actual parameters of designated transducers (Months 18-24).
c. Modify a state-of-the-art ultrasound imaging system to incorporate the ultrasound-activated contrast imaging modality (Months 21-24).
d. Evaluate the new imaging modality in an *in vitro* perfusion phantom using the modified ultrasound scanner (Months 21-24).

Task 3: To validate the clinical potential of ultrasound-activated contrast imaging using an established canine prostate cancer model (Months 25-32):

a. Create and grow prostate tumors by implanting a Canine Transmissible Venereal Sarcoma (CTVS) cell line into the prostate (Months 25-29).
b. Produce and evaluate activation-enhanced contrast images of canine prostates with CTVS tumors (Months 26-30).
c. Perform pathological evaluations of prostate specimens and quantify the microvessel density with immunohistochemical staining (Months 28-31).
d. Process data and images and write final report (Months 31-32)